J Comp Physiol A
DOI 10.1007/s00359-007-0275-1

ORIGINAL PAPER

Object localization through the lateral line system of fish: theory and experiment

Julie Goulet · Jacob Engelmann · Boris P. Chagnaud · Jan-Moritz P. Franosch · Maria D. Suttner · J. Leo van Hemmen

Received: 1 September 2006 / Revised: 3 September 2007 / Accepted: 16 September 2007

Abstract Fish acquire information about their aquatic environment by means of their mechanosensory lateral-line system. This system consists of superficial and canal neuromasts that sense perturbations in the water surrounding them. Based on a hydrodynamic model presented here, we propose a mechanism through which fish can localize the source of these perturbations. In doing so we include the curvature of the fish body, a realistic lateral line canal inter-pore distance for the lateral-line canals, and the surface boundary layer. Using our model to explore receptor behavior based on experimental data of responses to dipole stimuli we suggest that superficial and canal neuromasts employ the same mechanism, hence provide the same type of input to the central nervous system. The analytical predictions agree well with spiking responses recorded experimentally from primary lateral-line nerve fibers. From this, and taking into account the central organization of the lateral-line system, we present a simple biophysical model for determining the distance to a source.

Keywords Lateral line · Orientation · Distance · Hydrodynamic · Modeling · Neuromasts

Abbreviations

A/D	Analog to digital
CN	Canal neuromast
D	Distance perpendicular to the line of detectors
DASPEI	2-(4-(Dymethylamino)styryl-*N*-ethylpyridinium iodide
ERP	Extra-cellular receptor potential
SEM	Scanning electron microscopy
SN	Superficial neuromast
Δ	Distance between the zeros and/or distance between the maxima in the flow field
$\Delta_{\parallel}$	Distance between the zeros in the flow field
$\Delta_{\perp}$	Distance between the maxima in the flow field

Julie Goulet did the physical modeling and Jacob Engelmann was responsible for physiological measurements and justifications.

J. Goulet · J.-M. P. Franosch · M. D. Suttner · J. L. van Hemmen (✉)
Physik Department T35, TU München and
Bernstein Center for Computational Neuroscience,
85747 Garching bei München, Germany
e-mail: LvH@tum.de

J. Goulet
e-mail: julie@ph.tum.de

J. Engelmann
Institute of Zoology, University of Bonn,
Endenicher Allee 11-13, 53115 Bonn, Germany

B. P. Chagnaud
Institute of Zoology, University of Bonn,
Poppelsdorfer Schloss, 53115 Bonn, Germany

Introduction

Fish and many other aquatic vertebrates use a specific sensory system, the mechanosensory *lateral-line* system or for short the lateral line, to orient themselves by using hydrodynamic cues. In this work we focus on the question of how the lateral line enables fish to determine the spatial location of a stimulus in their aquatic environment. Our motivation for this work was to improve the general understanding of the biological physics governing the *interaction* between the lateral line and the water surrounding it by applying and solving the Navier–Stokes

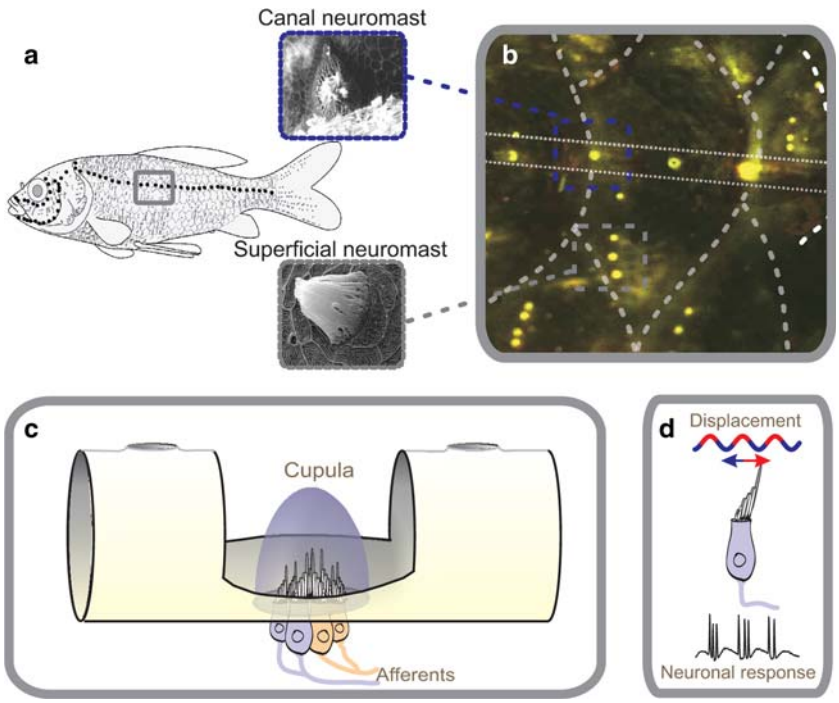

Fig. 1 Organization of canal and peripheral lateral-line system. **a** The distribution of canal pores (*small black disks*) and superficial neuromasts (*grey dots*) in goldfish (*Carassius auratus*); fish picture modified after A. Grotefeld. **b** Close-ups of SNs and CNs situated on the trunk of a goldfish. Neuromasts (*light dots*) are marked by the fluorescent dye DASPEI. The *insets* show SEM images of a single SN with cupula and a single CN. **c** Schematic of a CN embedded in the surrounding canal. The cupula and the two separately innervated populations of hair cells of opposite polarity are sensitive to either water moving from left to right or in the opposite direction. **d** Schematic of a sinusoidal stimulus used in the physiological experiments and its impact on a single hair cell

equation and in this way clarifying the mechanisms underlying the ensuing neuronal processing. We also vindicate the assumption that the Euler equation, although neglecting viscosity, is a valid starting point and, hence, we justify the approach of numerous preceding works in this field (Harris and van Bergeijk 1962; Sand 1981; Coombs et al. 1996; Franosch et al. 2005; Ćurčić-Blake and van Netten 2006), as discussed below.

The lateral line functions in a rather complex context with many different physical factors. These must be analyzed separately, in specifically defined behavioral contexts, in order to understand the underlying neuronal mechanisms involved in information processing and in the generation of the behavioral responses observed. We may expect, and also show, that both the curvature of the fish's body and the distance separating lateral line canal pores affect the responses of canal neuromasts (CN).

Having elucidated the underlying physics, we incorporate these factors into our model. In addition, we consider the boundary layer, a thin layer of fluid around any moving object where viscosity is essential. The behavior of this layer can be described by the Navier–Stokes equation. Although the Euler equation does not take fluid viscosity into account, it nevertheless effectively justifies a simple description of the stimulus once the boundary layer has been "added" to the fish body.

Based on our analysis of the fundamental stimulus properties we present a detailed investigation of the responses of lateral-line receptors within and outside the canals, the latter being the superficial neuromasts (SN), and reveal strong similarities between the two. We then compare modeling results and neuronal data.

Finally, we present a simple, though still putative, algorithm enabling fish to determine the distance to a source. This distance algorithm only depends on a single parameter that we confirm to be encoded in the neuronal response ensuing from both SN and CN of fish; cf. Fig. 1.

In summary, our aim has been to provide a detailed theoretical analysis of the biophysics and neurobiology of fish lateral-line detection, together with experimental analysis of the neural representation of known sensory images, in order to explain how the physical characteristics of the near-flow velocity and pressure field are translated as a neuronal code, and can then be embedded into a full hydrodynamic description of both fish and stimulus. Mutatis mutandis, many results also hold for SN of aquatic amphibians such as *Xenopus*.

Materials and methods

In this section we introduce both the theoretical and the experimental methods we are going to use. Experimental results and mathematical derivations will be presented in the next section.

Assumptions for a minimal model

To theoretically analyze a complicated situation, models with a minimal amount of assumptions are most useful. In the present context a "minimal" model means for the canal lateral-line system a straight line of detectors with equidistant pores and cupulae in between. More precisely, a detector is either sensitive to velocity (SN) or to the pressure difference between pores (CN), i.e., to acceleration. To approximate natural conditions we will consider both the case of a linear array of detectors and detectors that are arranged on a *curved* line, just as along the skin of a fish.

The simplest stimulus is a small moving sphere that generates a so-called dipole flow field as defined in Lamb (1932, Sect. 92). *Any* source can be expanded mathematically into a multipole series consisting of a monopole, a dipole, a quadrupole and so forth (Pozrikidis 1997). The quadrupole and higher terms are negligible as they rapidly decrease with distance. The monopole term, if at all present, is a sound wave that is only relevant far away from a source (Kalmijn 1988). Thus the dipole is the most important stimulus, which is easily realized experimentally by a small *vibrating* or *translating* sphere.

In simulations, the stimulus was a small vibrating or translating sphere at a distance D from CNs; see Fig. 2 for a sketch of the model. If not stated otherwise, the sphere has a diameter $a = 5$ mm, oscillates at frequency $f = 50$ Hz (angular frequency $\omega = 2\pi f$) and with a displacement amplitude $s = 0.8$ mm, or a translating sphere with velocity $U = 10$ cm/s.

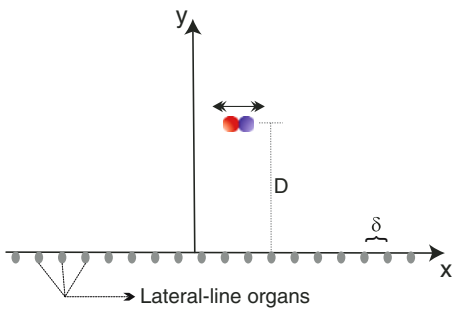

Fig. 2 In the 2-D *minimal* model, the lateral-line organs are arranged in a linear array on the x-axis. The distance between them and between two consecutive pores is taken to be δ. An oscillating sphere is located at position $(0,D)$. It oscillates parallel to the x-axis, generating a dipolar velocity field

In order to understand the fluid motion produced by these stimuli, we need to turn to the Navier–Stokes equation (Acheson 1990)

$$\frac{\partial \boldsymbol{v}}{\partial t} + (\boldsymbol{v}\cdot\nabla)\boldsymbol{v} = -\frac{\nabla p}{\rho} + \upsilon\Delta\boldsymbol{v} + \boldsymbol{g} \tag{1}$$

where υ is the water velocity, p the pressure, ρ the water density, $\boldsymbol{g}$ the acceleration of gravity, and υ the kinematic viscosity giving rise to the dissipative term $\upsilon\Delta\boldsymbol{v}$. The Navier–Stokes equation is supplemented by the incompressibility condition $\nabla\cdot\boldsymbol{v} = 0$ and the *no-slip* boundary condition $\boldsymbol{v}|_{\partial\mathcal{B}} = 0$, so that the fluid velocity vanishes at the body surface $\partial\mathcal{B}$. In fluids with low viscosity υ, such as water, viscosity only has an effect in a small *boundary layer* (Prandtl 1904; Schlichting and Gertsen 2003) which is at most 2–3 mm thick under the conditions considered here.

Outside the boundary layer the *Euler* equation applies, i.e., Eq. (1) with $\upsilon = 0$,

$$\frac{\partial \boldsymbol{v}}{\partial t} + (\boldsymbol{v}\cdot\nabla)\boldsymbol{v} = -\frac{\nabla p}{\rho} + \boldsymbol{g}. \tag{2}$$

Here the fluid motion is merely bounded by a wall, the boundary of a region $\mathcal{B}$ with normal vector $\boldsymbol{n}$, so that $\boldsymbol{n}\cdot\boldsymbol{v}|_{\partial\mathcal{B}} = 0$ is the appropriate boundary condition for the Euler equation.

As a first approximation, a SN responds to the velocity field whereas a CN reacts to the pressure difference between the two pores surrounding it, i.e., acceleration. Well, do they? It was Kalmijn (1988) who argued in favor of a fractional derivative (Sokolov et al. 2002) interpolating, so to speak, between velocity (first derivative with respect to time) and acceleration (second derivative). Though quite an interesting idea, there is not enough convincing evidence at present to introduce such a fit procedure. However, one cannot derive the parameter $1 < n < 2$ for the *fractional* derivative. Furthermore, we suppose, and nearly always observe, an average velocity $\boldsymbol{v}_0 \neq 0$ for our fish and can develop whatever quantity necessary with respect to deviations from $\boldsymbol{v}_0$. We will therefore remain with the traditional picture.

When dealing with CNs it is important to realize that the Navier–Stokes equation (1) governs the fluid dynamics *in* the canal whereas the pressure field *on the skin* of the fish can be described by the Euler approximation (2) since the perpendicular pressure is almost constant in the boundary layer near the skin (Schlichting and Gertsen 2003). The pressure difference between two adjacent pores is the relevant external force driving the fluid through the canal. In the canal, the water velocity is proportional to the *pressure difference* between two pores (Denton and Gray 1982). In contrast, a SN response is directly proportional to the water velocity near the skin of the fish.

The dipole flow field can be described by a velocity potential ϕ with $\upsilon = \nabla\phi$. For a sphere at position (D_x, D_y) that oscillates *parallel* to the x-axis and in the plane of the lateral-line organ (Fig. 2) with $\mu(t) := 2\pi\omega s a^3 \sin(\omega t)$ the two-dimensional (2-D) potential ϕ, as described in Lamb (1932, Sect. 92) is

$$\phi_{\parallel}(x,y,t) = \frac{-\mu(t)}{4\pi}\left\{\frac{(x-D_x)}{[(x-D_x)^2+(y-D_y)^2]^{3/2}} + \frac{(x-D_x)}{[(x-D_x)^2+(y+D_y)^2]^{3/2}}\right\}, \tag{3}$$

which satisfies the boundary condition $\upsilon \cdot n = 0$ of the Euler equation on the surface of the sphere. The resulting water velocity $\upsilon_x = \partial\phi_{\parallel}/\partial x$ in x-direction is

$$\upsilon_x(x, y=0, t) = \frac{\mu(t)}{2\pi}\frac{(2x^2-D^2)}{(x^2+D^2)^{5/2}}. \tag{4}$$

In the case of a sphere oscillating *perpendicularly* to the skin of the fish, i.e., in the direction of the y-axis (Fig. 2), we find[1]

$$\phi_{\perp}(x,y,t) = \frac{-\mu(t)}{4\pi}\left\{\frac{y-D_y}{[(x-D_x)^2+(y-D_y)^2]^{3/2}} - \frac{y+D_y}{[(x-D_x)^2+(y+D_y)^2]^{3/2}}\right\}. \tag{5}$$

The resulting water velocity $\upsilon_x = \partial\phi_{\perp}/\partial x$ in x-direction is

$$\upsilon_x(x, y=0, t) = \frac{3\mu(t)Dx}{2\pi(x^2+D^2)^{5/2}}. \tag{6}$$

Figure 3 shows the water velocity near the skin of the fish. In the case of parallel oscillation, the water velocity which is dependant on the position at the skin is an even function. In the case of perpendicular oscillation, the water velocity is an odd function. To use the symmetry of the water velocity in both cases, we normally set $D_x = 0$, $D = D_y$, $y = 0$ at the skin and let x vary between -5 and 5 cm.

The water velocity around the body of a fish stimulates the SNs. Relatively short in length (about 0.2 mm), they are affected by the boundary layer. In order to see how large the effect is, we have done a numerical simulation of a 2-D Navier–Stokes equation using Comsol (a numerical simulation software) and compared the results with a calculation using the Euler equation (Fig. 4).

We were only interested in the water flow *parallel* to the boundary since the flow perpendicular to the boundary layer decreases fast within the boundary layer. Using the method of images to satisfy the boundary conditions of the Euler equation, one can show that in the presence of a plane wall, the fluid velocity near and parallel to the wall will double; see for example Sect. 4.4 of Acheson (1990).

[1] The potential for an *arbitrary* axis of vibration in the xy-plane making an angle α with the x-axis is $\phi(x,y,t) = \phi_{\parallel}(x,y,t)\cos\alpha + \phi_{\perp}(x,y,t)\sin\alpha$.

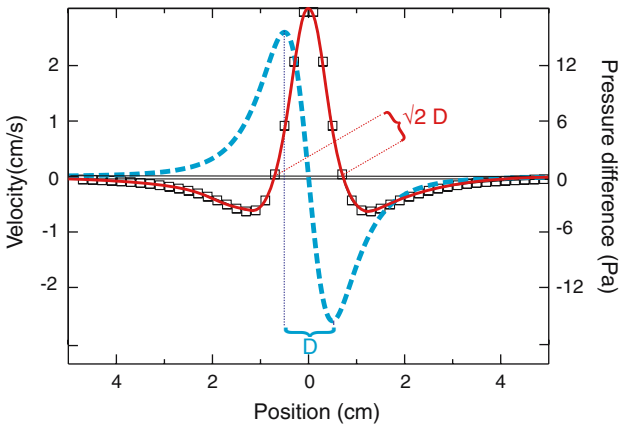

Fig. 3 Amplitude of the velocity υ_x near the skin of the fish in dependence upon the x-position. The stimulus is an oscillating sphere at $D = 1$ cm from the skin. The sphere is oscillating either *parallel* (*solid line*, cf. Eq. (4)) or *perpendicularly* (*dashed line*, cf. Eq. (6)) to the line of detectors and thus generates either a *tri*phasic or a *bi*phasic response. The distance between the zeros is $\sqrt{2}D$ for the *parallel condition* and the distance between maximum and minimum is D for the *perpendicular condition*. The *squares* represent the pressure difference. The velocity field and pressure difference field are *proportional* to each other; cf. Eq. (14)

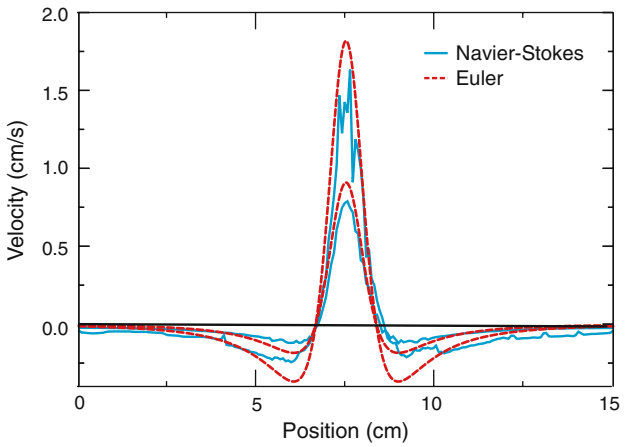

Fig. 4 x-Component of the velocity field v at 1 mm distance from the skin of the fish, modeled as a wall, for both the Navier–Stokes (*solid line*) and the Euler (*dashed line*) equation. Stimulus is a sphere oscillating in x-direction with frequency $f = 50$ Hz, sphere diameter $a = 5$ mm, and amplitude $s = 0.8$ mm at a distance of 1 cm from the wall (the *two upper curves*). The *two lower curves* are simulation results where the wall is missing. There are local fluctuations in the velocity field because of the viscosity of water, but the resulting dipole field has the same spatial characteristics as in the Euler case. The simulations show that the effect of the wall as predicted by the Euler equation (2), namely doubling the velocity, is also present in numerical simulations using the Navier–Stokes equation (1)

In the case of a *viscous* fluid the boundary condition of the Navier–Stokes equation prescribes that the velocity field vanishes at the wall. Numerical simulation of the fluid velocity at 1 mm from the wall, using the Navier–Stokes equation, also shows that fluid velocity parallel to a wall is *almost* twice the velocity produced by the same stimulus without a wall (Fig. 4). We therefore conclude that even within the boundary layer the flow *parallel* to the wall can be approximated by the Euler equation so that we can neglect the effect of the boundary layer.

Furthermore, the theoretical predictions Eq. (36) for the firing rate and the activity fields recorded at the primary afferents agree nicely as do predictions stemming from the Euler equation and the experimental results in Fig. 8; see "Results".

Experimental method

Details of fish maintenance, anesthesia, and preparation are given in Chagnaud et al. (2006).

Stimulation

Stimuli were generated by means of metal spheres (diameters 5, 8.7, 10, and 17 mm) attached to a vibrator (Ling, Model V101) via a stainless steel shaft. Sine waves (50 Hz, 100 ms rise and fall time, duration 1 s) were generated (Superscope II) and transferred via an A/D converter (MacAdios) to a custom made dB-attenuator whose output was fed to a power amplifier (LDS, PA 25 E) that drove the vibrator. The vibration axis of the sphere was always parallel to the long axis of the fish. The displacement amplitude of the sphere was calibrated in air with a microscope (Leitz, Laborlux K) and could be varied between 1 and 1,000 μm.

We determined the location of a neuromast by moving the vibrating sphere along the x-axis, maintaining the sphere's distance (y-position measured from the neuromast to the center of the sphere) and its elevation (z-position) constant. The x-position where the vibrating sphere evoked the strongest response was taken as the rostro-caudal position of the recorded neuromast. In the majority of the recordings the elevation of the sphere was optimized at this position so as to obtain the strongest response so that the final sphere position was directly opposite to the neuromast.

We then adjusted the y-distance of the sphere and the displacement amplitude to give a neural response below saturation rate (between 20 and 100 μm). Keeping these conditions constant we measured the receptive field, i.e., we determined the spatial extent over which the stimulus was able to evoke changes in the afferent discharge when moving the sphere along the x-axis. We moved the vibrator in steps of 2–10 mm along the x-axis and recorded the response to stimulation at each position (ten repetitions, repetition rate 0.5 Hz) over several centimeters. When possible, the receptive field was measured for various y-distances. In total we measured 60 receptive fields in 54 afferents of 26 fish.

Data analysis and recordings

We recorded and analyzed the evoked primary afferent firing activity by means of standard procedures; see Engelmann et al. (2002) for details. For each x-position of the vibrating sphere we measured the firing rate due to the vibrating sphere and the spontaneous rate in absence of stimulation (spikes/s), the phase of the neuronal response with respect to the phase of the vibrating sphere (degrees) and the degree of phase-coupling (r-value, Batschelet 1981). The statistical significance of phase-coupling was assessed by the Rayleigh Z statistic (Goldberg and Brown 1969).

Figure 5 shows this data as so-called "receptive field" plots. On the trunk of the fish there are two orientations of receptors (Schmitz et al. 2006). One orientation is sensitive to flow in the x-direction (Fig. 2) and the other orientation is sensitive to flow perpendicular to the x-direction. In the former case the receptive field plot is characterized by three peaks of the evoked discharge-rate that are separated by two 180° phase shifts (*triphasic* response, see Fig. 5a) while in the latter case there are two consecutive peaks of the evoked discharge-rate which are separated by a 180° phase shift (*biphasic* response, see Fig. 5b) (Sand 1981; Coombs et al. 1996).

Thirty-nine afferents were classified as triphasic and 15 as biphasic (only CN); cf. Fig. 5. For triphasic receptive fields we take the distance between two consecutive phase shifts as the physiological realization of the distance between the zeros of the velocity field. For biphasic receptive fields the distance between the peaks of the discharge rate corresponds to maximum and minimum, i.e., maximum with opposite direction, of the velocity field; see Figs. 3 and 5.

Results

In the following we present the modeled hydrodynamic stimuli for SNs and CNs, including an experimental proof of the modeled results. We address the parameters required for distance determination in both the modeled and the physiological data.

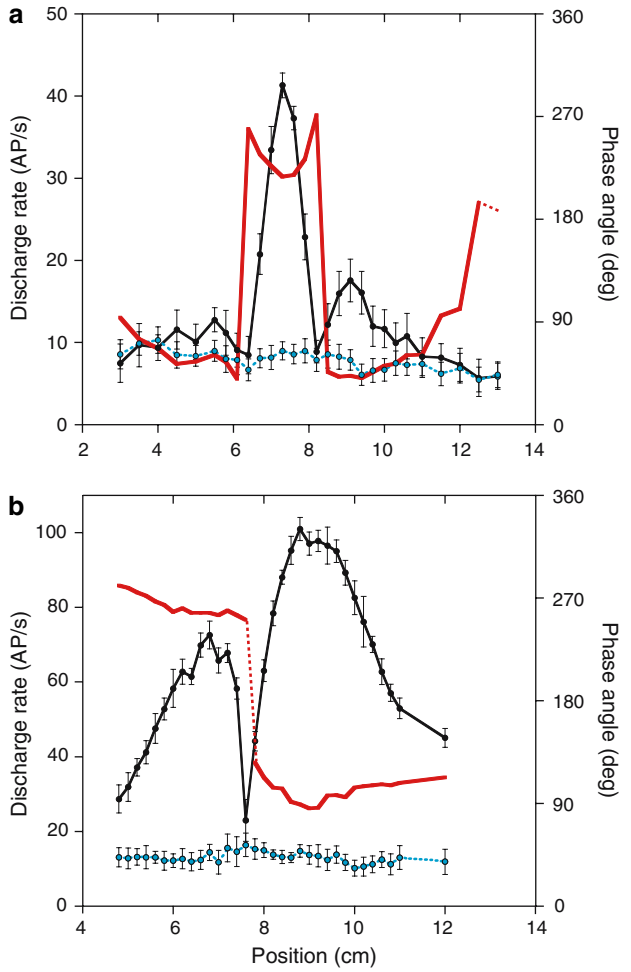

Fig. 5 Physiological parameters recorded as a function of sphere position for triphasic (**a**), and biphasic (**b**) receptive field. In both figures the mean (n = 10 trials) discharge rate (*solid line and circle*) and the ongoing discharge rate (*dashed line and circle*) have been plotted (y-axis on the *left*) versus the sphere's position. *Error bars* show standard deviations. Mean phase angles are plotted in *thick solid lines* (cf. y-axis on the right). Non-significant phase locking ($Z < 4.6$) is indicated by the *dotted lines*. In **a** the sphere vibrated at a rate of 50 Hz, with 80 μm sphere displacement and distance 15 mm to the neuromasts (trout). In **b** the distance was 25 mm and the amplitude was 200 μm (goldfish). In *triphasic* receptive fields (**a**) for oscillations parallel to the lateral line the distance $\Delta_{\parallel}$ between the zeros was determined to be the distance between the two 180° phase jumps; cf. Fig. 1. In *biphasic* receptive fields (**b**) for oscillations perpendicular to the lateral line the distance $\Delta_{\perp}$ between the zeros was taken to be the distance between the two consecutive peaks of the discharge rate

Distance determination by superficial neuromasts

How can fish determine the position of *small* sources?

Surface neuromasts are sensitive to the velocity (change) in the direction of their primary axis. The velocity is zero at the two points where fluid motion reverses; see Fig. 3. For a translating or vibrating sphere near SNs (Franosch et al. 2005) and a vibrating sphere near CNs (Ćurčić-Blake and van Netten 2006) the distance Δ between the two zeros (or the two maxima/minima) is a measure of the distance between object and fish. Here we extend these ideas and in essence show that Δ is *proportional to* the distance between the lateral line and a *vibrating* sphere for SNs for an axis of vibration parallel as well as perpendicular to the skin of the fish.

In case of oscillation parallel to the lateral-line the velocity in the x-direction is given by Eq. (4). In view of $\mu(t) = 2\pi\omega s\ a^3 \quad \sin(\omega t)$; the velocity oscillates with frequency f, i.e., angular frequency $\omega = 2\pi f$, around a maximum value of

$$v_{x-\max}(x, y = 0) = \frac{\omega a^3 s(2x^2 - D^2)}{(x^2 + D^2)^{5/2}}. \tag{7}$$

Equation (7) has two zeros. The distance between the two zeros, which we will denote by $\Delta_{\parallel}$, is

$$\Delta_{\parallel} = \sqrt{2}D. \tag{8}$$

Thus the distance between the zeros of the velocity field is proportional to the distance D of the sphere to the skin *and does not depend on any other parameter*.

For a sphere oscillating *perpendicularly* to the skin the velocity field is given by Eq. (6). The amplitude of this flow field along the lateral line has two maxima separated by a zero. The distance between the maxima equals the distance D between the lateral line and the oscillating sphere

$$\Delta_{\perp} = D. \tag{9}$$

It is interesting to see that the above results are similar to those derived by Ćurčić- Blake and van Netten (2006) in the context of CNs.

Distance determination by canal neuromasts

Canal neuromasts are sensitive to the pressure difference between two adjacent pores. We are therefore interested in the pressure field and will show analytically that the pressure difference distribution along the lateral line canal has a form *identical* to the velocity field. For distance determination this means that both SNs and CNs function by the same mechanism.

To calculate the pressure in a *non*-viscous fluid at the pores of the canal lateral line, we can use the Bernoulli equation (Billingham and King 2000)

$$\left[p(x, y, t) + \frac{1}{2}\rho v^2(x, y, t) + \rho\frac{\partial\phi_{\parallel}}{\partial t}\right]_{y=D} = p_0(t) \tag{10}$$

where v^2 is the square of the water flow velocity at the body and $p_0(t)$ is a constant depending on the time t only. Since the velocity $v_y = \partial\phi_{\parallel}/\partial y$ perpendicular to the skin is zero

at the skin because of the Euler boundary condition, we find $v^2 = v_x^2$. Using Eq. (3) for a sphere at distance D from the skin oscillating parallel to the x-axis we get

$$v^2(x, y = 0, t) = v_x^2 = \left(\partial\phi_\parallel/\partial x\right)^2 = \frac{a^6\omega^2 s^2(2x^2 - D^2)^2}{(x^2 + D^2)^5}\sin^2(\omega t). \quad (11)$$

Again, the notion of a *thin* boundary layer is important since outside of this layer we can use the Euler and Bernoulli equations to obtain the pressure. It holds that $\partial_t\phi_\parallel \gg v^2$.

The time derivative ∂_t of the velocity potential for an oscillating sphere is

$$\frac{\partial\phi_\parallel(x, y, t)}{\partial t} = \frac{1}{2\pi}\frac{\mathrm{d}\mu(t)}{\mathrm{d}t}\frac{x}{(x^2 + D^2)^{3/2}} \quad (12)$$

where $\mathrm{d}\mu(t)/\mathrm{d}t = 2\pi\omega^2 a^3 s \cos(\omega t)$. The water velocity within the canal and thus the deflection of the CNs is proportional to the pressure difference Δp between two adjacent pores at position (x,y = 0) on the skin

$$\Delta p(x, y = 0, t, \delta) = \frac{\partial\phi_\parallel(x + \delta, 0, t)}{\partial t} - \frac{\partial\phi_\parallel(x, 0, t)}{\partial t} \quad (13)$$

where δ is the distance between the pores. As δ is small, we obtain

$$\Delta p(x, y = 0, t, \delta) \approx \frac{\partial}{\partial t}\frac{\partial\phi_\parallel(x, y = 0, t)}{\partial x}\cdot\delta = \omega v_{x-\max}(x, y = 0)\cos(\omega t)\cdot\delta. \quad (14)$$

In general, using Eq. (3) we get

$$\Delta p(x, y = 0, t, \delta) = -\omega^2 a^3 s\rho\left[\frac{\delta + x}{\left((\delta + x)^2 + D^2\right)^{3/2}} - \frac{x}{(x^2 + D^2)^{3/2}}\right]\cos(\omega t). \quad (15)$$

Figure 3 shows a plot of the maximum amplitude of $\Delta p(x,y = 0,t,\delta)$ as a function of x for $\cos(\omega t) = -1$. It reveals that the pressure difference distribution has a form *identical* to the velocity field. Again the distance between the zeros $\Delta_\parallel$ is proportional to the distance D of the sphere. A mathematical expression for the distance between the zeros can be found by equating Eq. (15) to zero and then keeping only the terms linear in δ since $\delta \ll x$ and $\delta^2 \ll \delta$. This leads to

$$-2D^6 + 6D^2x^4 + 4x^6 = 0. \quad (16)$$

The above equation has two real-valued zeros $x = \pm D/\sqrt{2}$. Hence $\Delta_\parallel = \sqrt{2}D$, which corresponds to what we have shown before for the velocity field governing the response of SNs.

Angle determination

Franosch et al. (2005) have shown that for a translating sphere the angle α (angle between the axis of vibration of the sphere and the x-axis) can be determined from the zeros and the maxima and minima of the flow field. This is possible for *any* α.

Real fish, however, may use a special behavioral strategy based on the zeros, since the latter are easily detectable. In experiments on blind mottled sculpins it was observed that fish frequently approaches the source in a step-wise manner (Schwartz and Hasler 1966; Conley and Coombs 1998; Coombs 1999). First they align themselves parallel to the axis of the sphere motion where $v(x)$ is an even function of the position; see Fig. 3. Second, they approach the sphere frontally. These two steps are repeated at increasingly closer distances until the fish is close enough for a strike. Based on this approach behavior, we assume that the fish measures the position of a vibrating sphere when the trunk lateral line is *parallel* to the direction of vibration. This behavioral mechanism solves the problem of angle determination.

Angle-determination algorithm for angles near 0 and $\pi/2$ have been proposed previously (Franosch et al. 2005; Ćurčić-Blake and van Netten 2006). In addition, Franosch et al. (2005) have also presented a relation valid for any angle. At the moment, however, it is difficult to select a universal mechanism that fish use. We therefore limit ourselves to the case of a stimulus moving in *parallel* or *perpendicularly* to the skin of a fish.

Three dimensions

There is evidence (Janssen et al. 1990) that fish can use their lateral line not only to detect a source in a *horizontal* plane but also to determine the source's *elevation*, i.e., its z-component. Anatomical data show that both SNs and CNs are organized orthogonal to each other (Schwartz and Hasler 1966). In the following we show how fish could compute the *3-D* position of a dipole from lateral-line data.

For a dipole at position (0, D_y, D_z), we get

$$\phi_\parallel(x, y, z, t) = -\frac{\mu(t)}{4\pi}\left\{\frac{x}{\left[x^2 + (D_y - y)^2 + (D_z - z)^2\right]^{3/2}} + \frac{x}{\left[x^2 + (D_y + y)^2 + (D_z - z)^2\right]^{3/2}}\right\}. \quad (17)$$

Simplifying the anatomy of the lateral line, we assume two lines of receptors arranged perpendicular to each other along the x and z-axis (with y = 0), so as to get

$$v_x = \frac{\mu(t)}{2\pi}\frac{2x^2 - [(D_y)^2 + (D_z - z)^2]}{\left[x^2 + D_y^2 + (D_z - z)^2\right]^{5/2}}. \quad (18)$$

Since we are interested in the velocity along the line of receptors on the x-axis, we set z to zero and calculate the distance between the zeros as

$$\Delta_{3D} = \sqrt{2}(D_y^2 + D_z^2)^{1/2}. \quad (19)$$

For the line of receptors along the z-axis we find

$$v_z = \frac{\mu(t)}{2\pi}\frac{3x(D_z - z)}{[x^2 + D_y^2 + (D_z - z)^2]^{5/2}}. \quad (20)$$

If $x \neq 0$ (i.e., the line of detectors is not at $x = D_x = 0$) then there is one point with zero velocity the z-axis at $z = D_z$.

The fish may then determine the position of a dipole in three dimensions as follows. The x-position D_x of the dipole is between the two zeros of v_x. The z-position D_z is at the zero of v_z. The y-position is calculated with Eq. (19). We have done the above calculation for receptors sensitive to velocity, i.e., SNs. For CNs the same calculation applies since we have already shown through Eq. (14) that the pressure difference distribution along the canal lateral line has an identical form to that of the velocity field.

Translating sphere

The velocity field due to a *translating* sphere is a dipole (Lamb 1932). SNs can encode the distance to such a source (Franosch et al. 2005). Here we show that the localization mechanisms we have presented above are also applicable to the detection of a translating sphere by means of the CNs. Say, a sphere is moving in the x-direction with velocity w and starting point x_0 at time $t = 0$. Then the distance in the x-direction between a CN at position x and the sphere at time t is

$$X(t,x) = x - (x_0 + wt). \quad (21)$$

The velocity potential is

$$\phi_{\parallel}(x,y,t) = 2a^3 w\left\{\frac{X(t,x)}{[X(t,x)^2 + (y - D)^2]^{3/2}} + \frac{X(t,x)}{[X(t,x)^2 + (y + D)^2]^{3/2}}\right\}. \quad (22)$$

Due to the Bernoulli equation (10) we find

$$p(x,y,t) - p_0(t) = -\rho\left[\frac{1}{2}\left(\frac{\partial\phi}{\partial x}\right)^2 + \frac{\partial\phi}{\partial t}\right]. \quad (23)$$

Since the second term is dominant, the pressure difference between two consecutive pores is approximately

$$\Delta p(x,t) \approx \frac{\mathrm{d}}{\mathrm{d}x}\frac{\partial\phi_{\parallel}(x,y,t)}{\partial t}\bigg|_{y=0}\cdot\delta \quad (24)$$

where δ is the distance between two pores. Using (22) we arrive at

$$\begin{aligned}\Delta p(x,t) &= 2a^3 w^2\delta\frac{\partial^2}{\partial^2 X}\frac{X(t,x)}{[X^2(t,x) + D^2]^{3/2}} \\ &= 6a^3 w^2\delta\frac{X[2X^2(t,x) - 3D^2]}{[D^2 + X^2(t,x)]^{7/2}}.\end{aligned} \quad (25)$$

This field is *anti*symmetric in x and the distance between its maximum and minimum is $\Delta_{\parallel} = 0.72\ D$.

In the case of a sphere translating *perpendicularly* to the line of detectors we have

$$D(t) = D_0 + wt. \quad (26)$$

The velocity potential is

$$\phi_{\perp}(x,y,t) = 2a^3 w\left\{\frac{y - D(t)}{[x^2 + [y - D(t)]^2]^{3/2}} - \frac{y + D(t)}{[x^2 + [y + D(t)]^2]^{3/2}}\right\}. \quad (27)$$

Therefore the pressure difference (15) between two pores becomes

$$\Delta p(x,t) \approx \frac{\mathrm{d}}{\mathrm{d}x}\frac{\mathrm{d}\phi_{\perp}(x,y,t)}{\mathrm{d}t}\bigg|_{y=0}\cdot\delta = 6a^3 w^2\delta\frac{4D^2(t)x - x^3}{[D^2(t) + x^2]^{7/2}}. \quad (28)$$

The pressure difference field is again antisymmetric in x and the distance between the maximum and the minimum is $\Delta_{\perp} \approx \sqrt{1.21}D$. Hence a simple linear encoding of the distance between fish and object may well hold for a translating sphere too.

Extending the minimal model to a lateral line with curvature

So far we have modeled the lateral-line system as a straight line. Strictly speaking, this may be, and in general is, incorrect since a fish body is practically always curved. We have therefore applied our method to a curved surface in order to analyze the effect of curvature on the relationship between the zeros of the velocity field and pressure difference field. Because of curvature the relation between the distance $\Delta_{\parallel}$ of the zeros and the distance of the sphere becomes non-linear. We note, however, that this relation is always *independent* of the dipole strength, which means that the distance to the sphere can nevertheless be computed from the distance between the zeros. We will also quantify the effect of curvature for two real goldfish.

To determine the effect of curvature on a line of SNs as well as CNs, we measured the shape of two goldfish (6.5 and 10 cm long). Assuming the fish is axially symmetric with respect to the x-axis, we use a polynomial to fit the geometry of the fish. Let $Y(x)$ be the distance of the fish's skin from the x-axis. As shown in Fig. 6, a polynomial of degree three of the form $Y(x) = a\,x^3 + b\,x^2 + c\,x + d$ can already fit the experimental data. Table 1 shows the coefficients.

The dipole is at distance D from the fish's skin and at x-position X_0. Here the skin is at distance $Y_0 := Y(X_0)$ from the x-axis. For a sphere oscillating parallel to the tangent to the (now curved) line of detectors the velocity potential at position $(x, Y(x) + y)$ is

$$\phi_{\parallel}(x,y,t) = \frac{-\mu(t)}{4\pi}\left\{\frac{x-X_0}{\left\{[x-X_0]^2+[y-D+Y(x)-Y_0]^2\right\}^{3/2}} + \frac{x-X_0}{\left\{[x-X_0]^2+[y+D-Y(x)+Y_0]^2\right\}^{3/2}}\right\}. \tag{29}$$

The distance $r(x)$ between the point at position x on the lateral line and the center of the oscillating sphere is

$$r(x) = \left\{[x-X_0]^2 + [D-Y(x)+Y_0]^2\right\}^{1/2}. \tag{30}$$

With the definition

$$R(x) := \left\{[x-X_0]^2 + Y^2(x)\right\}^{1/2} \tag{31}$$

the velocity field at the fish's skin ($y = 0$) is

$$\begin{aligned} v_x(x,t) &= \frac{1}{R(x)}\frac{\partial\phi_{\parallel}(x,y,t)}{\partial x}\bigg|_{y=0} \\ &= \frac{1}{R(x)}\left\{\frac{\partial\phi_{\parallel}[x,Y(x),t]}{\partial x} + \frac{\partial\phi_{\parallel}[x,Y(x),t]}{\partial Y}\frac{\mathrm{d}Y(x)}{\mathrm{d}x}\right\}_{y=0} \\ &= \frac{\mu(t)}{4\pi R(x) r^5(x)}\{2[x-X_0]^2 - [D-Y(x)+Y_0]^2 \\ &\quad + 3[x-X_0][D-Y(x)+Y_0][\mathrm{d}Y(x)/\mathrm{d}x]\}. \end{aligned} \tag{32}$$

The zeros of the velocity field follow from $v_x(x,t) = 0$ and therefore from

$$2[x-X_0]^2 - [D-Y(x)+Y_0]^2 + 3[x-X_0][D-Y(x)+Y_0]\,[\mathrm{d}Y(x)/\mathrm{d}x] = 0. \tag{33}$$

The distance between the two *real* zeros (x_+ and x_-) along the fish's skin is

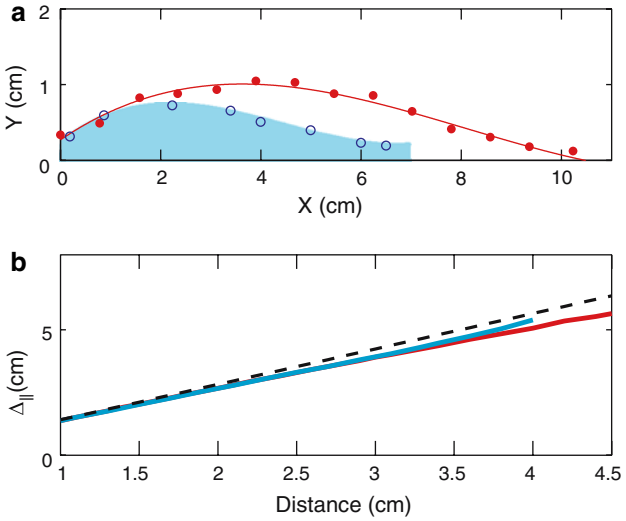

Fig. 6 **a** Experimental measurement of the curvature and, thus, of the radius of curvature of two real goldfish (*open circle* 6.5 cm long, *filled circle* 10 cm long). The *solid line* represents a polynomial fit to the data; see Table 1 for the coefficients. **b** The theoretical distance $\Delta_{\parallel}$ between the zeros in the velocity field for the two goldfish as a function of the distance D to the sphere. The *black dashed line* is the approximation $\Delta_{\parallel} = \sqrt{2}D$ valid for a straight lateral line. There is only a small difference between both fish. Moreover, Eq. (34) shows that $\Delta_{\parallel}$ *only* depends on the distance to the stimulus and not on stimulus amplitude or frequency

Table 1 Polynomial fit through $a\,x^3 + b\,x^2 + c\,x + d$ for the radius of curvature of two *real* goldfish

Length of the fish (cm)	a	b	c	d
6.5	0.012	0.16	0.53	0.22
10	0.0033	0.08	0.45	0.27

Figure 6a shows that such a polynomial of degree 3 already fits the experimental data quite well

$$\Delta_{\parallel} = \int_{x_-}^{x_+} \sqrt{1 + |\mathrm{d}Y(x)/\mathrm{d}x|^2}\,\mathrm{d}x. \tag{34}$$

Figure 6b shows that the difference in $\Delta_{\parallel}$ between the two goldfish is negligible. Figure 9a compares the theory developed above with experimental results.

In the case of a dipole oscillating *perpendicularly* to the line of detectors, we proceed in the same way except that we are now focusing on the difference between the maxima of the velocity amplitude instead of the zeros.

The velocity field on the skin of the fish is

$$v_x(x,t) = \frac{-\mu(t)}{4\pi R(x)}\left\{\frac{3[x-X_0][D-Y(x)+Y_0] + r^2(x) - 9[x-X_0][D-Y(x)+Y_0]}{r^5(x)}\right\}. \tag{35}$$

The distance $\Delta_\perp$ between the maxima of the velocity amplitude follows from $dv_x/dx = 0$. The zeros of the velocity field, i.e., $v_x(x,t) = 0$, do not depend of $\mu(t)$ and therefore the distance D to the dipole is just a function of the distance to the source and the form of the fish body.

Figure 7 shows for a circular lateral line the speed at which $\Delta_\parallel$ and $\Delta_\perp$ converge to the values for a straight line. It shows that the effect of curvature is not negligible for bigger fish. The Appendix contains the mathematical derivation.

Comparison between modeled and measured data

In this section we test the theoretical predictions by comparing them with recordings from lateral-line nerve fibers. As shown in previous studies, the two observed patterns can be predicted by the amplitude and direction of the pressure gradients surrounding a dipole source for a vibration axis that is either parallel (trimodal pattern) or orthogonal (bimodal pattern) to the orientation of the pores (Sand 1981; Coombs et al. 1996, 1998; Coombs and Conley 1997b).

Some *general* predictions of our model have been confirmed by experimental data as well. A prediction of all analytic models is that the distance $\Delta_\parallel$ between the zeros in the velocity *and* pressure fields is only a function of stimulus distance and hence independent of the sphere displacement amplitude, size, and frequency; cf. Eq. (8). Various sphere sizes and amplitudes were tested in two cases and neither sphere size nor vibration amplitude had an effect on $\Delta_\parallel$ (data not shown); for the dependence upon the amplitude see also Ćurčić-Blake and van Netten (2006).

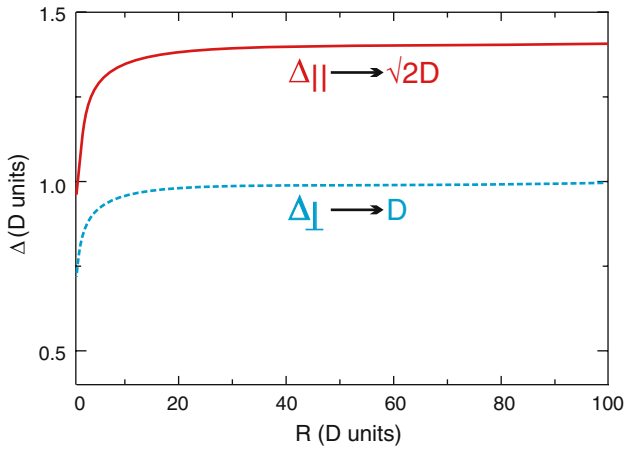

Fig. 7 Effect of decreasing curvature R^{-1} as the radius of curvature R becomes large so that $R^{-1} \to 0$. The distance $\Delta_\parallel$ between the zeros of the velocity field converges to $\sqrt{2}D$ (*solid line*) for a parallel direction of oscillation of the sphere. In case of perpendicular oscillations the distance $\Delta_\perp$ between the maxima in amplitude of the velocity field converges to D (*dashed line*)

To determine the degree of agreement between the theoretic predictions and the measured responses, we compare a "firing rate" function of the form (triphasic field)

$$F(x) = \left| I + A \frac{[2(x-x_0)^2 - D^2]}{[(x-x_0)^2 + D^2]^{5/2}} \Theta \right| \tag{36}$$

with actual receptive fields. Here I is the experimentally determined instantaneous firing rate, A denotes a scaling parameter and x_0 is the position of the sphere. The variable Θ is 1 when the neuronal response is in phase with the vibrating sphere and -1 when there is a 180° phase difference; cf. Fig. 5.

In the case of a sphere moving perpendicularly to the skin of the fish (biphasic field), the firing rate is

$$F(x) = \left| I + A \frac{D(x-x_0)}{[(x-x_0)^2 + D^2]^{5/2}} \Theta \right|. \tag{37}$$

As shown in Fig. 8, the agreement between the modeled firing rate F and the three arbitrarily chosen neuronal receptive fields is quite good.

Determining distance

We now turn to the question of whether, and how, the distance to the sphere is unambiguously encoded in the distance between the zeros or the maxima in the discharge pattern of the afferents. Since our model shows that the factor governing the linear relationship between sphere distance D and Δ depends on the orientation of the neuromasts, we first present the results obtained by pooling data from afferents with identical orientations. For "triphasic" fibers Fig. 9a shows the dependence of the distance $\Delta_\parallel$ between the zeros of the velocity field upon the distance D to the sphere. For "biphasic" fibers Fig. 9b shows the dependence of the distance $\Delta_\perp$ between the amplitude maxima upon D.

A linear fit of the data shows that there is a correlation between the distance to the sphere and the distance between the phase reversals for the case of triphasic receptive fields with $\Delta_\parallel \approx 1.13\, D$ ($R^2 = 0.96$). The slope of this fit is significantly larger than 1 and smaller than $\sqrt{2}$. The model including the curvature of the fish explains the measured data better. The obtained slope is thus in good agreement with the two values predicted by a linear model for both SNs and CNs. It is important to note that neuronal data for this analysis were not sorted by neuromast type (CN or SN) but only by the orientation of the neuromasts (triphasic or biphasic receptive field).

Since the linear relation between Δ and D is just an approximation valid for a *flat* fish we also show the

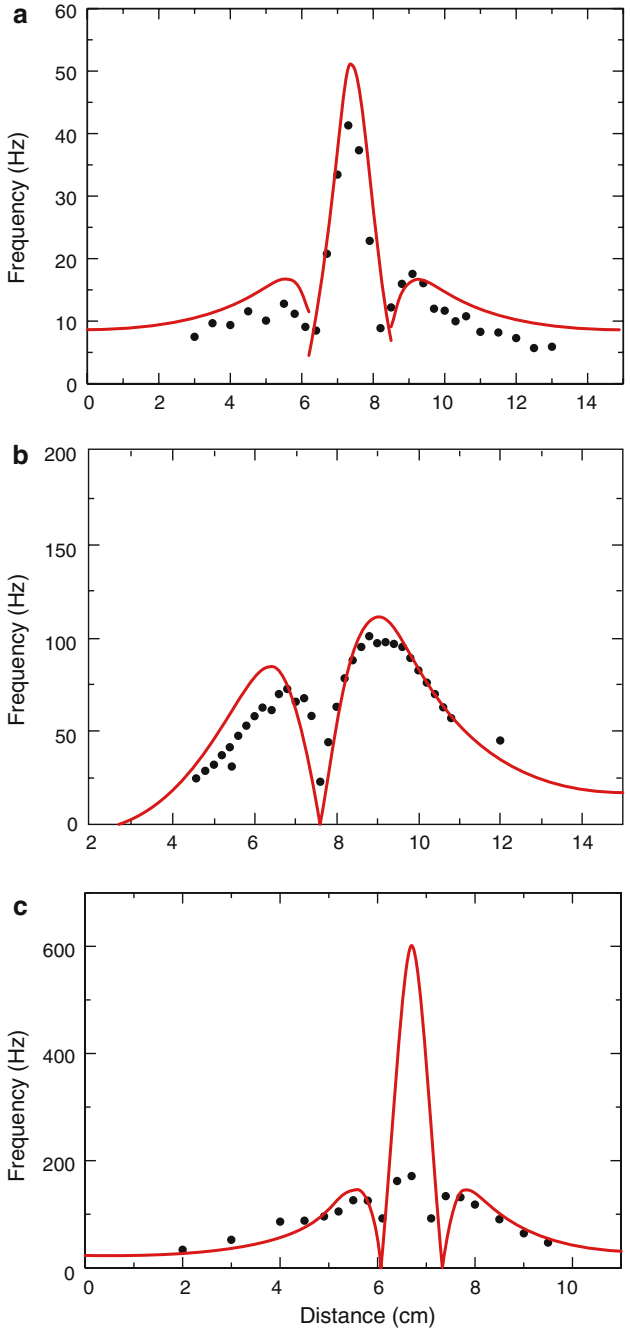

Fig. 8 Experimentally measured firing rates (*black dots*, mean of ten stimuli) at afferent nerve fibers and theoretical predictions (*solid lines*) of Eqs. (36) and (37). **a** A triphasic field of a *CN* for an oscillating sphere at distance $D = 1.5$ cm from the skin of the fish, instantaneous firing rate $I = 8$, and the free parameter $A = 170$ to fit the amplitude. **b** A biphasic field for a sphere at distance $D = 2.6$ cm from the skin of the fish, $I = 13$ and $A = 6{,}000$. **c** A triphasic field of a *superficial* neuromast for an oscillating sphere at distance $D = 0.93$ cm, $I = 13$ and $A = 500$. In this case, the difference between theory and experiment is *probably* related to rate saturation (see "Discussion")

theoretical results in the case of a *real* fish. For the biphasic case $\Delta_\perp = 1.02D$, which is not significantly different from the slope 1.0 given by Eq. (9).

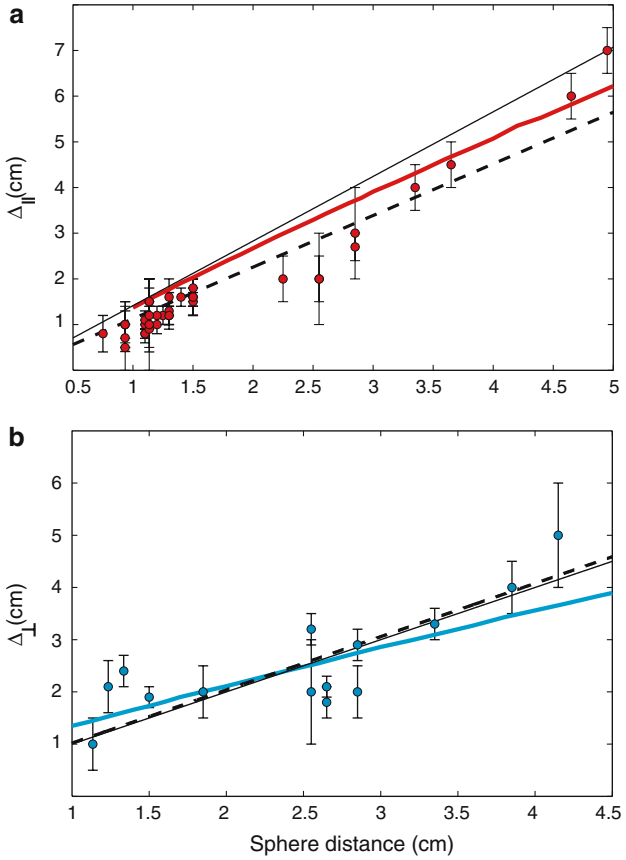

Fig. 9 **a** Distance $\Delta_{\parallel}$ between the zeros of the velocity field as a function of sphere distance for afferents with triphasic receptive fields. *Error bars* show standard deviations in *y*-direction. The standard deviation in *x*-direction is 0.1 cm. The *thick solid line* is the theoretic prediction for the curved 10 cm long goldfish; cf. and Eq. (33). The *dashed line* is the predicted result for a straight lateral line; cf. Eq. (8). The *thin solid line* is the best linear fit of the measured data 1.13 *D*. The data agree well with the theoretical prediction for the curvature effect. **b** Distance $\Delta_\perp$ between the maxima in amplitude of the velocity field as a function of sphere distance for afferents with biphasic receptive fields. The *thick solid line* is the theoretic prediction for the curved 10 cm long goldfish. The *dashed line* is the predicted result for a straight lateral line Eq. (9). The *thin straight line* 1.02 *D* is the best linear fit to the measured data. The horizontal axis is the sphere distance *D* in both cases (**a** and **b**)

We did not attempt to separate CNs and SNs here. The physiological data confirm the results shown in Fig. 3, i.e., both the velocity and the pressure difference between the pores present the distance of the sphere in the *same* manner. This was further confirmed when we analyzed the receptive fields of triphasic SNs and CNs separately (Fig. 10). There is no significant difference in the slope for the CNs and the SNs population.

Discussion

In view of the multifaceted aspects of our results we will list and discuss them in turn. Throughout this paper and

hence also throughout what follows we focus on *dipolar* stimuli such as an oscillating or uniformly translating small sphere or, for instance, a small fish swimming in the neighborhood of an adult pike.

For a discussion of results it is useful to first put things into a historical perspective. Lateral line analysis has a long history culminating in a first review by Dijkgraaf (1963); see also the great collection of essays in Coombs et al. (1989), in particular, those by Kalmijn and Hassan, the detailed mathematical analysis due to Hassan (1985, 1992a, b, 1993), and Bleckmann's succinct monograph (Bleckmann 1994) evenly combining biological data and mathematical description.

There are also several studies addressing questions similar to those analyzed here, starting with Harris and van Bergeijk (1962) and Sand (1981), continuing with Coombs et al. (1996) and most recently, Franosch et al. (2005) and Ćurčić-Blake and van Netten (2006). Though Coombs and co-workers (Coombs 1994, 1999; Coombs et al. 1996, 2000, 2001; Coombs and Conley 1997a, b; Conley and Coombs 1998) have analyzed an impressive collection of data, we are facing several, partially inconsistent, conclusions. The inconsistency is mainly due to the fact that these authors have not analyzed the *physics* of the problem in sufficient detail. Their insight, however, that *only* the *near* flow field can communicate outside information to the lateral line has certainly stimulated a lot of recent work.

Franosch et al. (2005) were the first to unequivocally show that the distance between the zeros or between maxima and minima of the velocity field encode the spatial distance D between an aquatic stimulus and fish. In particular, the distance between *characteristic* lines of the velocity field on the fish body scales with D with a prefactor of order 1. If, for instance, fish would encode the distance D to a prey by the distance between maxima and minima of the near flow field, scaling with D, then they need to be able to *detect* both maximum and minimum. However, if D is too large, exceeding fish length, then the information is to be incomplete. Encoding D is no longer possible, and hence distance determination in higher brain centers is no longer possible either. These points concerning the maxima and minima would hold equally well for the two zeros of the dipolar velocity field; see below. This natural explanation of the "short" range of the lateral-line system as "about one fish length" in fact justifies a criterion that has been known to biological tradition since long; (Harris and van Bergeijk 1962, Sand 1981). Though the above theoretical evidence was quite compelling, physiological evidence for a sharp estimate in terms of the near-flow field was still missing.

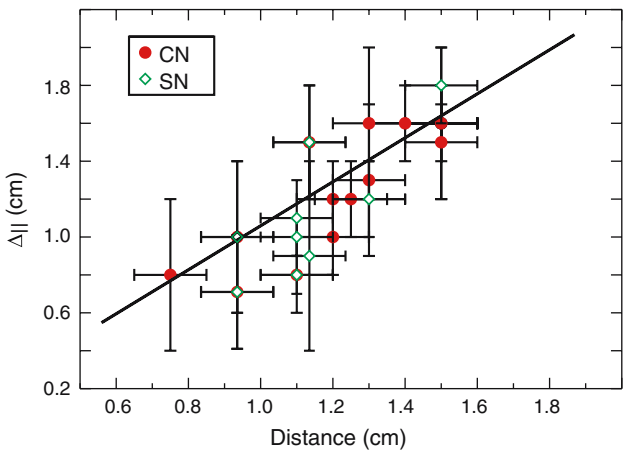

Fig. 10 Distance $\Delta_{||}$ as a function of sphere distance for *CNs* ($n = 15$) and *SNs* ($n = 10$) with triphasic receptive fields, i.e., cells sensitive to motions along the x-axis. The 25 samples stem from a population of 17 goldfish and 8 trout. *Error bars* represent standard deviations in x-direction. The plot confirms the theoretical prediction that *both CNs and SNs* encode distance on the same way, since the populations are small and the error bars important, we are not able to make definitive conclusion about the value of the slope for a linear relation. The *black line* $y = x$ is therefore just a guide to the eye

Analyzing extracellular receptor potentials (ERPs), also called microphonic potentials, which arise from the collective mechano-transduction of hair cells in single neuromasts, Ćurčić-Blake and van Netten (2006) showed that the above criterion of zeros of the velocity field scaling with D indeed holds for ERPs, thus providing a first experimental confirmation of this theoretically attractive idea. On the other hand, their interpretation of the ERP data in terms of a wavelet read-out is somewhat questionable since it is unclear why, and how, fish should use such a complicated mathematical procedure, if things also work simply and straightforwardly in biological terms, a key result of the present paper.

Canal and superficial neuromasts are equivalent

Canal and superficial neuromasts are the two types of neuromast relevant to the lateral line functioning in fish. By carefully analyzing the hydrodynamics underlying the biophysical detection mechanisms giving rise to the response of both we have arrived at the rather surprising conclusion that both operate through the *same* mechanism so that ensuing neuronal procedures need not discern the input of CNs and SNs, and can handle both identically, cf. Fig. 3 and Eq. (14). We now turn to the hydrodynamics through which such a mechanism becomes operational.

Our finding that both SNs and CNs employ the same encoding scheme for determining the distance to a dipolar source agrees with what is known about the projections present in the lateral-line system. While it has been demonstrated that there is a proof of a crude somatotopic representation of the lateral-line in goldfish (Kröther et al.

2001) and the zebra fish brain (Alexandre and Ghysen 1999), there is no evidence that afferents of SNs or CNs project to distinct areas in the *Medulla*. Recordings from central neurons in the *Medulla*, where input from the primary afferent is further processed, show that information about the zero-distances of the near-flows velocity fields can be maintained at this level (Mogdans and Kröther 2001). The fact that such neurons exist in the initial stage of information processing suggests that the actual extraction of the distance Δ between the zeros (or maxima/minima) of the near-flow velocity field may well occur higher up in the sensory system.

Behavioral support for the hypothesis that both CNs and SNs being involved in distance estimation comes from experiments on the Mottled sculpin (*Cottus bairdi*) showing that these fish can locate a vibrating sphere even if the CNs are mechanically blocked (Janssen and Corcoran 1998). Nevertheless, the CNs are necessary (Coombs et al. 2001) for an *efficient* distance determination, although juvenile sculpins, which possess SNs only, can orient themselves towards small copepods (Janssen et al. 1987).

Localization: determining distance

Hydrodynamic images are to some extent comparable to visual images. With increasing distance image become blurred (O'Shea et al. 1994, 1997; Maher 1997) and this can be used in monocular vision for distance determination. In contrast to visual images, however, hydrodynamic images lack a lens adjusting the focus. Consequently hydrodynamic images get wider with increasing distance while visual images in fact get smaller as the distance increases. For our data this translates into the finding that the distance between the maxima and minima or zeros of the velocity field of a dipole increase monotonically with the distance to the source; cf. Figs. 3, 6, 9 and 10 and Eqs. (8) and (9). Hence the knowledge of this relationship may well suffice for a fish to determine the distance to predator, prey, or conspecifics—at least as long as the latter can be described as oscillating dipoles or moving spheres. Another argument for localization based on distance between the zeros or the maxima and minima of the near-flow velocity field (cf. Figs. 3, 5) is that the spatial location of these points is *invariant* in time so that it enables quicker localization than if complete reconstruction of the stimuli were required over a period of time, say an oscillation period, is nearly always in the range of 30 Hz and below, the times we need to think of exceed 30 ms.

Both Coombs et al. (1996) and Coombs and Conley (1997b) already noted that there is a relation between the distance D to a dipole and the width Δ between the phase-reversals in the receptive fields of primary afferents. These authors did not investigate, however, this relation quantitatively. A more detailed investigation for the SNs of *Xenopus* has been presented recently by Franosch et al. (2005) and for the CNs of the ruff by Ćurčić-Blake and van Netten (2006). As we have seen, a natural consequence of Δ's scaling with D, is in fact a fundamental restriction depending on what part of the lateral-line system we focus on, e.g., trunk, mouth, or eyes, is that the range of the respective parts of the lateral-line system is about one fish length, the width of the mouth, or the eye diameter. From a biological point of view, this makes a lot of sense.

Even more importantly, though Eqs. (33) and (34) show that because of the curvature of the fish body the relation encoding the distance is in general *non*-linear, it is independent of dipole strength and the speed of a translating sphere. In other words, though curvature makes the relation between the distance D to a sphere and the Δ between zeros or maximum/minimum of the near-flow velocity field non-linear, the relation is a function of the distance and some *internal* parameters, such as the form of the fish, *only*. Thus fish can learn to evaluate the distance without considering any other external parameter. This is relevant since considerable curvature often occurs at the head of a fish, in particular, for neuromasts situated around the mouth and the eyes. On the other hand, the effect of curvature is rather moderate for small distances; for example, for a small prey near an adult pike. We therefore conclude that in many cases even a simple linear algorithm may well suffice to determine distance.

In passing we note that our simple 'minimal' model is based on an arrangement of neuromasts in a plane. That is, for a flat fish. Quite often this is a reasonable approximation of the trunk lateral line. Including curvature alters the results originating from the simple model as described by Eq. (34). However, it does not alter the essence of our result that lateral-line neuronal input encodes the distance of a dipole independently of its intensity.

The above facts suggest that "distance-neurons" might exist in the ascending lateral-line system, although it is unlikely that distance tuning, in the sense of a one-to-one neuron coding, is established in the system. Future experiments should address the question of whether central lateral-line neurons show tuning characteristics related to distance and whether this tuning can be related to the zeros-distance or min/max parameter Δ.

Localization in *three* dimensions

Extending our findings that similar coding strategies are employed by SNs and CNs to orientation in 3-D space, we propose that fish can determine distance to and elevation of a source either by the aid of CNs arranged orthogonally to

each other, as one can frequently see on the fish head (Schwartz and Hasler 1966; Webb 1989a, 1989b; Faucher et al. 2003, 2005), or by a similar combination of SNs and CNs or SNs alone, as in *Xenopus* (Franosch et al. 2003, 2005). In either configuration—see Eq. 17)—two perpendicular lines of detectors are sufficient to extract the exact position of any source, provided that each line of receptors is long enough. In future behavioral experiments, it might be interesting to test for differences in the distance determination capability between fish that differ in lateral-line geometries or between fish of different sizes. In the latter case, where the density of neuromasts for many fish decreases with growth (Janssen and Corcoran 1998), one might expect a decrease in distance determination performance during development, as Jones and Janssen (1992) have indeed reported.

An oscillating dipole is effectively a 3-D construct in that its dipole moment is a 3-D vector. Velocities associated with fish are in general so small that one can take the Stokes approximation of the Navier–Stokes equation (1) and hence drop the non-linear term $v^2 \cdot \nabla v$, which is proportional to v^2. The remaining problem being linear we can decompose the dipole moment $\boldsymbol{p}$ into three components, one parallel to the long axis of the fish, a case we have treated extensively, and two directions orthogonal to it; say, with decomposition coefficients β_ι and $1 \leq \iota \leq 3$. The general solution to the velocity field is then a linear superposition of these three cases with exactly the same coefficients β_ι.

Wavelets could of course also be used to describe the pattern due to many dipoles pointing in different directions (Ćurčić-Blake and van Netten 2006). The problem, however, with the wavelet approach is that, although it makes it possible to reconstruct a complicated pattern one can measure, it gives no idea as to how fish analyze a single pattern through a general wavelet decomposition nor how they can neuronally segregate composite signals coming from many dipoles. This is open to future experiments but might well be more a problem of signal integration than one of pattern formation at the nerves. There is no evidence either that neurons perform pattern segmentation through a wavelet algorithm. Pattern segmentation is certainly an interesting topic; e.g., the model of Franosch et al. (2003) allows *Xenopus* to segregate a superposition of up to at least three sources generating *surface* waves, which has been confirmed recently by experiment (Elepfandt, private communication). This kind of result is not available yet for *underwater* stimuli, i.e., for 3-D localization.

Shape of the fish body

In 3-D space the fish body has a finite extent. To arrive at exact results that provide insight we have to confine ourselves to specific shapes such as ellipsoids or perform an approximating series expansion (Handelsman and Keller 1967; Geer 1975). The algorithm developed here for an ellipsoid can be adapted by a weighting function that would adjust for the local degree of curvature. However, the error in distance estimation due to curvature may be negligible within the range of precision needed. For example, Janssen and Corcoran (1998) has shown that mottled sculpins tend to underestimate the source distance. As argued by the same author (Janssen 2004), it is probably not critical for the lateral-line mediated orientation system to be so precise. The sculpin still successfully captures its prey, even if the distance has not been estimated accurately, because the prey is ingested by means of a suction mechanism (Wainwright and Day 2007). Just getting close enough to the prey suffices to enable successful capture, at least for this fish. Precision may well be species-dependent.

Boundary layer

The notion of boundary layer is closely related to the shape of any object in an aquatic surroundings. It was already Prandtl (1904)—for details see Schlichting and Gertsen (2003)—who suggested more than a century ago that, if velocity is low, viscosity can be neglected and one can use the Euler equation (2) outside fish body with boundary layer. The latter's extent is typically 2–3 mm. Though we may then consider fish and boundary layer as one object, it is precisely the boundary layer where both SNs are found and from which the CNs get their information. As we have seen, for an incompressible fluid such as water the pressure perpendicular to the boundary layer is almost constant so that the boundary layer effectively plays no role. Moreover, the difference between the predicted and measured responses for the case shown in Fig. 8c is probably due to rate-saturation, as primary afferents do not discharge faster than at a rate of about 200 Hz.

Based on the numerical simulations, we have shown that the boundary layer can be neglected for both SNs and CNs. For SNs the point is that the spatial form of the field is maintained within the boundary layer. Hence both SNs and CNs detect dipole-like sources in the very same way. It is consequently not necessary to solve all possible problems related to hydrodynamics since instead it suffices to analyze far simpler configurations on the basis of the physical insights presented in this paper.

An interesting issue that deserves consideration in the present context is our finding that both velocity and pressure difference at the pores are increased in amplitude by interaction with the fish (or whatever) body. For instance, the factor of 2 that we have explained in the context of Fig. 4 was already noticed, though not understood, by

Hassan (1993) in his numerical simulations. Apart from the physical importance of the above result, it may also be of behavioral relevance. In a series of elegant experiments, Hassan (1986, 1989) also showed that *blind* Mexican cave fish can determine the structure of artificial surfaces as they glide past an object by using their highly developed lateral-line system.

In conclusion, by taking into account and carefully modeling the physical essentials underlying neuronal object localization as performed by the lateral line in an aquatic environment we can finally understand a bedazzling wealth of data and, what is equally important, see that they all belong to a grand, biologically and physically, consistent context.

Acknowledgments We gratefully acknowledge Hendrik Hagedorn's help with the analysis of the boundary layers of CNs. We also cordially thank Professor Horst Bleckmann for use of experimental facilities. Julie Goulet is supported by the Bernstein Center for Computational Neuroscience, Munich. Boris Chagnaud was supported by a grant from DARPA to Prof. Bleckmann and by the DFG (Bl 242/10-1). This project has been partially funded by the European Commission, Future and Emerging Technologies (CILIA). We especially thank Dr. Kirsty Grant and Ms Jeanne McRee for her extensive revision of parts of the manuscript. The experiments reported in this paper comply with the current animal protection law of the Federal Republic of Germany ("Tierschutzgesetz") as well as with the "Principles of animal care", publication no. 86-23, revised 1985 of the National Institute of Health.

Appendix: Convergence of the curved model

Another interesting question concerns the rate at which the predictions of the model describing a curved fish body converge to those of a straight line as the body curvature vanishes. In order to answer this question, we assume an arc of radius R at a distance D to an oscillating dipole. For a dipole oscillating parallel to the tangent to the curved line of detectors, the velocity potential is

$$\phi_{\parallel}(R,\theta,t) = \frac{-\mu(t)}{4\pi}\frac{R\sin\theta}{[R^2\sin^2\theta + (D+R-R\cos\theta)^2]^{3/2}} \tag{38}$$

where R is the radius of the lateral line, (0,D) the position of the dipole, and θ is the angle between the radius and the y-axis. The velocity in θ-direction (perpendicular to r) is

$$v_\theta(R,\theta) = -\frac{\mu(t)}{2\pi}\frac{2(D+R)^2\cos\theta + R(D+R)[\cos(2\theta)-5]}{2[(D+R-R\cos\theta)^2 + R^2\sin^2\theta]^{5/2}} \tag{39}$$

so that $v_\theta = 0$ results in

$$2(D+R)^2\cos\theta + R(D+R)[\cos(2\theta)-5] = 0. \tag{40}$$

Solving (40) explicitly for θ we find as real solutions

$$\theta_\pm = \mp\arccos\left[\frac{(D^2+2DR+2R^2)}{2R(D+R)} - \frac{(D^4+4RD^3+20R^2D^2+32R^3D+16R^4)^{1/2}}{2R(D+R)}\right]. \tag{41}$$

For small curvature, R is large. Focusing on the immediate surroundings of a dipole we assume θ is small and develop the expression in (40) into a Taylor series near $\theta = 0$,

$$2D^2 - (D+2R)^2\theta^2 + \mathcal{O}(\epsilon^4) = 0, \tag{42}$$

and find the solutions $\theta_\pm = \pm\sqrt{2}D/(D+2R)$ and hence $\Delta = (\theta_+ - \theta_-)R = 2\sqrt{2}DR/(D+2R)$. Since $D + 2R \approx 2R$ for large R we recover $\Delta = \sqrt{2}D$. Plotting $\Delta_\parallel = R(\theta_+ - \theta_-)$, we see from Fig. 7 that for a curvature near $R = D = 1$ cm the distance between the zeros is almost D, whereas for a straight lateral line the limit approaches $\sqrt{2}D$.

The same kind of solution is applicable for the *anti-symmetric* field. In this case the velocity potential is

$$\phi_\perp(R,\theta,t) = \frac{-\mu(t)}{4\pi}\frac{D+R(1-\cos\theta)}{\{(R\sin\theta)^2 + [D+R(1-\cos\theta)]^2\}^{3/2}}. \tag{43}$$

The maxima/minima of the velocity v_θ are at

$$\theta_\pm = \pm\frac{D\sqrt{2(2D+3R)}}{\sqrt{2D^3+16RD^2+37R^2D+24R^3}}. \tag{44}$$

The Taylor series as in Eq. (42) is

$$(-8D^4 - 12RD^3) + (4D^4 + 32RD^3 + 74R^2D^2 + 48R^3D)\,\theta^2 = 0. \tag{45}$$

Figures 6 and 7 show the dependence of the distance between the zeros or the maxima and minima of the velocity upon the distance to the stimulus. The distance $\Delta_\perp$ converges a bit faster to D than $\Delta_\parallel$. The above calculations show how a fish can localize objects in front of its mouth or eyes where curvature is of great importance.

References

Acheson D (1990) Elementary fluid dynamics. Oxford University Press, Oxford

Alexandre D, Ghysen A (1999) Somatotopy of the lateral line projection in larval zebra fish. Proc Natl Acad Sci USA 96:7558–7562

Batschelet E (1981) The Rayleigh test. In: Batschelet E (ed) Circular statistics in biology. Academic, New York, pp 54–58

Billingham J, King A (2000) Wave motion. Cambridge University Press, Cambridge

Bleckmann H (1994) Reception of hydrodynamic stimuli in aquatic and semiaquatic animals. In: Rathmayer W (ed) Sensory biology of aquatic animals, vol 44. Gustav Fischer, New York

Chagnaud BP, Bleckmann H, Engelmann J (2006) Neural responses of goldfish lateral line afferents to vortex motion. J Exp Biol 209:327–342

Conley RA, Coombs S (1998) Dipole source localization by mottled sculpin. III. Orientation after site-specific, unilateral denervation of the lateral line system. J Comp Physiol A 183:335–344

Coombs S (1994) Nearfield detection of dipole sources by the goldfish (*Carassius aurus*) and the mottled sculpin (*Cottus bairdi*). J Exp Biol 190:109–129

Coombs S (1999) Signal detection theory, lateral-line excitation patterns and prey capture behavior of mottled sculpin. Anim Behav 58:421–430

Coombs S, Conley RA (1997a) Dipole source localization by mottled sculpin. I. Approach strategies. J Comp Physiol A 180:387–399

Coombs S, Conley RA (1997b) Dipole source localization by the mottled sculpin. II. The role of the lateral line excitation patterns. J Comp Physiol A 180:401–415

Coombs S, Görner P, Münz H (eds) (1989) The mechanosensory lateral line: neurobiology and evolution. Springer, New York

Coombs S, Hastings M, Finneran J (1996) Modeling and measuring lateral line excitation patterns to changing dipole source locations. J Comp Physiol A 178:359–371

Coombs S, Mogdans J, Halstead M, Montgomery J (1998) Transformation of peripheral inputs by the first-order lateral line brainstem nucleus. J Comp Physiol A 182:606–626

Coombs S, Finneran JJ, Conley RA (2000) Hydrodynamic image formation by the peripheral lateral line system of the Lake Michigan mottled sculpin, *Cottus bairdi*. Phil Trans R Soc Lond B 355:1111–1114

Coombs S, Braun CB, Donovan B (2001) The orienting response of Lake Michigan mottled sculpin is mediated by canal neuromasts. J Exp Biol 204:337–348

Ćurčić-Blake B, van Netten SM (2006) Source location encoding in the fish lateral line canal. J Exp Biol 209:1548–1559

Denton E, Gray JAB (1982) The rigidity of fish and patterns of lateral line stimulation. Nature 297:679–681

Dijkgraaf S (1963) The functioning and significance of the lateral-line organs. Biol Rev Camb Philos Soc 38:51–105

Engelmann J, Hanke W, Bleckmann H (2002) Lateral line reception in still- and running water. J Comp Physiol A 188:513–526

Faucher K, Aubert A, Lagardere J (2003) Spatial distribution and morphological characteristics of the trunk lateral line neuromasts of the sea bass (*Dicentrarchus labrax*, L.; Teleostei, Serranidae). Brain Behav Evol 62:223–232

Faucher K, Lagardere JP, Aubert A (2005) Quantitative aspects of the spatial distribution and morphological characteristics of the sea bass (*Dicentrarchus labrax* L.; Teleostei, Serranidae) trunk lateral line neuromasts. Brain Behav Evol 65:231–243

Franosch J-MP, Sobotka MC, Elepfandt A, van Hemmen JL (2003) Minimal model of prey localization through the lateral-line system. Phys Rev Lett 91:1581011–1581014

Franosch J-MP, Sichert AB, Suttner MD, van Hemmen JL (2005) Estimating position and velocity of a submerged moving object by the clawed frog *Xenopus* and by fish—a cybernetic approach. Biol Cybern 93:231–238

Geer J (1975) Uniform asymptotic solutions for potential flow about a slender body of revolution. J Fluid Mech 67:817–827

Goldberg J, Brown PB (1969) Response of binaural neurons of dog superior olivary complex to dichotic tonal stimuli: some physiological mechanisms of sound localization. J Neurophysiol 32:616–636

Handelsman R, Keller J (1967) Axially symmetric potential flow around a slender body. J Fluid Mech 28:131–147

Harris GG, van Bergeijk JD (1962) Evidence that the lateral line organ responds to near-field displacements of sound sources in water. J Acoust Soc Am 34:1831–1841

Hassan ES (1985) Mathematical analysis of the stimulus for the lateral line organ. Biol Cybern 52:23–36

Hassan ES (1986) On the discrimination of spatial intervals by the blind cave fish (*Anoptichthys jordani*). J Comp Physiol A 159:701–710

Hassan ES (1989) Hydrodynamic imaging of the surroundings by the lateral line of the blind cave fish *Anoptichthys jordani*. In: Coombs S, Görner P, Münz H (eds) The mechanosensory lateral line: neurobiology and evolution. Springer, New York, pp 217–227

Hassan ES (1992a) Mathematical description of the stimuli to the lateral line system derived from a three dimensional flow field analysis: I. The case of moving in open water and of gliding toward a plane surface. Biol Cybern 66:443–452

Hassan ES (1992b) Mathematical description of the stimuli to the lateral line system derived from a three dimensional flow field analysis: II. The case of gliding alongside or above a plane surface. Biol Cybern 66:453–461

Hassan ES (1993) Mathematical description of the stimuli to the lateral line system derived from a three-dimensional flow field analysis: III. The case of an oscillating sphere near the fish. Biol Cybern 69:523–538

Janssen J (2004) Lateral line sensory ecology. In: von der Emde G, Mogdans J, Kapoor BG (eds) The sense of fish adaptations for reception of natural stimuli. Narose Publishing House, New Delhi, pp 231–264

Janssen J, Corcoran J (1998) Distance determination via the lateral line in the mottled sculpin. Copeia 1998:657–661

Janssen J, Coombs S, Hoekstra D, Platt C (1987) Anatomy and differential growth of the lateral line system of the mottled sculpin, *Cottus bairdi* (Scorpaeniformes: Cottidae). Brain Behav Evol 30:210–229

Janssen J, Coombs S, Pride S (1990) Feeding and orientation of mottled sculpin, *Cottus bairdi*, to water jets. Environ Biol Fish 29:43–50

Jones W, Janssen J (1992) Lateral line development and feeding behavior in the mottles sculpin *Cottus bairdi* (Scorpaeniformes: Cottidea). Copeia 1992:485–492

Kalmijn AJ (1988) Hydrodynamic and acoustic field detection. In: Atema J, Fay RR, Popper AN, Tavolga WN (eds) Sensory biology of aquatic animals. Springer, New York, pp 83–130

Kröther S, Mogdans J, Bleckmann H (2001) Projection patterns of lateral line nerve branchlets on the head and trunk of the goldfish, *Carassius auratus*. Proceedings of the 6th International Congress of Neurethology, Bonn, Germany, p 199

Lamb H (1932) Hydrodynamics, 6th edn. Cambridge University Press, Cambridge

Maher G (1997) The use of image blur as a depth cue. Perception 26:1147–1158

Mogdans J, Kröther S (2001) Brainstem lateral line responses to sinusoidal wave stimuli in the goldfish, *Carassius auratus*. Zoology 104:153–166

O'Shea RP, Blackburn SG, Ono H (1994) Contrast as a depth cue. Vis Res 34:1595–1604

O'Shea RP, Govan DG, Sekuler R (1997) Blur and contrast as pictorial depth cues. Perception 26:599–612

Pozrikidis C (1997) Introduction to theoretical and computational fluid dynamics. Oxford University Press, New York

Prandtl L (1904) Über Flussigkeitsbewegung mit kleiner Reibung. In: Verhandlungen des III. Internationalen Mathematiker-Kongresses, Heidelberg, 8–13 August 1904, Teubner, Leipzig, pp 484–491

Sand O (1981) The lateral line and sound reception. In: Tavolga WN, Popper AN, Fay RR (eds) Hearing and sound communication in fishes. Springer, New York, pp 459–480

Schlichting H, Gertsen K (2003) Boundary layer theory. Springer, Berlin

Schmitz A, Bleckmann H, Mogdans J (2006) Array morphology of the lateral line in goldfish *Carassius auratus*. 99th Annual meeting of the German Zool. Soc., Münster

Schwartz E, Hasler AD (1966) Superficial lateral line sense organs of the mudminnow. Z vergl Physiol 53:317–327

Sokolov IM, Klafter J, Blumen A (2002) Fractional kinetics. Phys Today 55(11):48–54

Wainwright PC, Day SW (2007) The forces exerted by aquatic suction feeders on their prey. J R Soc Interface 4:553–560

Webb J (1989a). Gross morphology and evolution of the mechano-receptive system in teleost fishes. Brain Behav Evol 33:34–53

Webb J (1989b) Neuromast morphology and lateral line trunk canal ontogeny in two species of cichlids: an SEM study. J Morphol 202:53–68